



Numerical study of degradation of fluvial hanging valleys due to climate change

Joseph K. Goode¹ and Douglas W. Burbank¹

Received 10 December 2007; revised 6 October 2008; accepted 7 November 2008; published 13 February 2009.

[1] Hanging fluvial valleys form at mouths of tributaries that are unable to incise as quickly as the trunk stream. Although hanging valleys at tributary mouths are uncommon, in very rapidly eroding ranges, such as the Himalaya, they can attain heights of ~ 1 km and display mean channel slopes exceeding 30° . Given a hypothesis based on bed load–saltation erosion for how such features form, this study addresses the question of why hanging valleys are not more common and what limits their growth. We implement a numerical model of bed load–saltation erosion for a tributary junction experiencing base-level fall to explore conditions that may lead hanging valleys to form or subsequently degrade owing to climate variability. We find that increased frequency of bed load mobilization and enhanced bed load supply can drive the degradation of hanging fluvial valleys. Moreover, when trunk aggradation overtops the hanging valley, the knickpoint tends to be removed during subsequent degradation of the alluvial surface. Channel narrowing, increased bed load size, or bed load supply each can inhibit the formation of hanging fluvial valleys. Under steady hydrological and sedimentologic conditions, bed load–saltation models predict hanging valleys could be quite common where main stem erosion is rapid. The frequency and magnitude of changes in climatically modulated sediment loads in natural systems, however, typically overwhelm factors that promote hanging valley formation without such bed load variability. Because rates of channel aggradation commonly outpace rates of hanging valley formation, we propose that hanging valleys tend to be preserved only in regimes where trunk-stream erosion exceeds several millimeters per year.

Citation: Goode, J. K., and D. W. Burbank (2009), Numerical study of degradation of fluvial hanging valleys due to climate change, *J. Geophys. Res.*, 114, F01017, doi:10.1029/2007JF000965.

1. Introduction

[2] Hanging valleys created by fluvial processes represent oversteepening of tributary channels near their junctions with higher-order streams [Wobus *et al.*, 2006]. Unlike most knickpoints in channel profiles, the steepened channel reach does not migrate significantly upvalley over time [cf. Bishop *et al.*, 2005; Whipple, 2004], but remains approximately pinned to the tributary-main stem junction. Whereas knickpoints are commonly 1.2 to 2 times steeper than adjacent reaches, hanging valleys can be more than 10 times steeper than adjacent upstream tributary reaches or the main stem that they join, such that waterfalls and cascades near the tributary mouth are juxtaposed with channels displaying much lower slopes. In the context of a fall in relative base level, hanging fluvial valleys form because a tributary channel is unable to keep pace with the rate of downcutting in the main stem channel [Crosby *et al.*, 2007]. If this mismatch in rates is

maintained over time, steepened tributary reaches can grow in height to hundreds of meters.

[3] Hanging fluvial valleys have recently been described from the Central Range of Taiwan [Wobus *et al.*, 2006] in a region where thermochronologic studies suggest erosion rates of 2–6 mm/a [Willett *et al.*, 2003]. The steepened reaches at tributary mouths reach 500 m in height and occur most commonly in catchments that flow directly into the sea, suggesting that eustatic sea level change might promote formation of these hanging valleys. Hanging valleys also occur in the central Himalaya where erosion rates are rapid: generally exceeding 3 mm/a [Blythe *et al.*, 2007; Whipp *et al.*, 2007]. Along the Marsyandi River in central Nepal, longitudinal profiles and data on channel slopes versus catchment areas that were extracted from a 90-m DEM reveal numerous hanging valley tributaries with steepened reaches at their mouths (Figure 1). Whereas some steepened reaches are up to 1 km high, others are only a few 10s of meters in height and are confined closely to the tributary junction. Nonetheless, as the Marsyandi traverses the Greater Himalaya, hanging valleys are almost ubiquitous. Of the 14 tributaries that are less than 10% of the main stem size in this reach (Figure 1), thirteen are significantly steepened immediately above their confluence with the main stem in comparison to the channel

¹Department of Earth Science, University of California, Santa Barbara, California, USA.

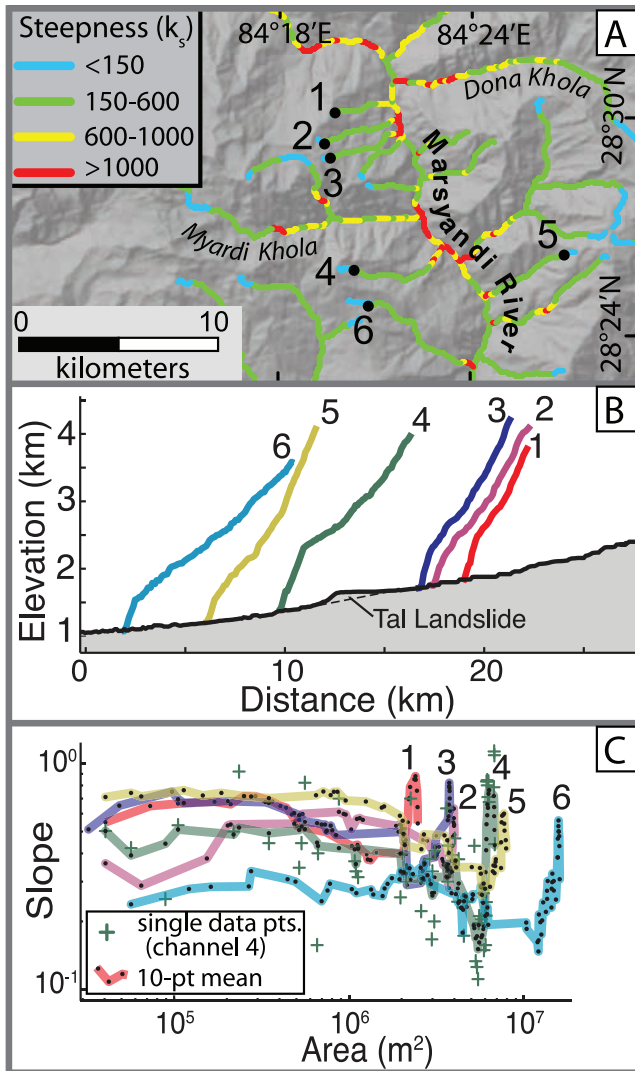


Figure 1. Hanging fluvial valleys in the central Nepalese Himalaya. (a) Shaded relief 90-m DEM map of the Marsyandi River network within the Greater Himalaya with color-coded steepness indices. Note the Marsyandi catchment drains >2000 km² upstream of this region. Normalized steepness indices, k_s (defined by $k_s = S A^{-\theta}$, where S is slope, A is catchment area, and $\theta = 0.45$ [Whipple, 2004]), indicate zones of pronounced steepening ($k_s \geq 600$) near the mouth of many tributary channels. (b) Long profiles of hanging valleys and the main stem Marsyandi channel. Note steepenings as high as 1 km where channel slopes approach 45° . Numbers refer to labeled channels in Figure 1a. (c) Channel slope versus catchment area plots of the hanging valleys above. Lines depict 10-point running means. Note the threefold to eightfold steepening near the tributary junction. Individual data points (crosses) for profile 4 are also shown. Data were extracted using programs from <http://geomorphtools.org>.

steepness farther up the tributary. Overall, these hanging valleys are situated well below the glacial limit [Duncan *et al.*, 1998; Pratt-Sitaula, 2005] and lie ~ 1000 km from the coast, such that neither glaciation nor eustatic variability can have played a direct role in their formation. As seen with the Taiwan examples, the Nepalese hanging tributaries (1) dis-

play order-of-magnitude increases in channel steepness just upstream of their junction with main stem channels and (2) tend to occur in tributary catchments that are more than ten times smaller than the main stem (Figure 1). Although steepening of river profiles is known to occur across reaches where differential rock uplift is more rapid [Cowie *et al.*, 2006; Kirby and Whipple, 2001; Lavé and Avouac, 2001], such localized differential uplift does not appear to be associated with hanging valleys in Taiwan or the Himalaya, given that these valleys tend to be oriented parallel to, rather than across, known gradients in rock uplift (Figure 1).

[4] In most landscapes, hanging fluvial valleys are uncommon or are associated with contrasts in rock resistance. Knickpoints, however, are more abundant, particularly in tectonically active landscapes, where they are typically interpreted as either a transient, upstream-migrating response to a change in the rate of relative base-level lowering or as a “steady-state” adjustment to variations in differential rock uplift along a channel [Kirby and Whipple, 2001; Lavé and Avouac, 2001]. The goal of this contribution is to explore potential reasons why the preservation of hanging valleys appears to be uncommon. Given numerical predictions that fluvial and tectonic conditions in rapidly eroding settings commonly favor the formation of hanging valleys, what factors limit their growth and preservation? Because the bed load incision rule of Sklar and Dietrich [2004] is unique among commonly applied bedrock-river incision rules in its ability to predict the formation of hanging fluvial valleys [Crosby *et al.*, 2007], we use this equation to model an incipient hanging fluvial valley at a tributary junction. This same description of channel erosion is then used to predict how fluvial hanging valleys may degrade owing to changes in climatically controlled model parameters. We explore the sensitivity of tributary erosional capability to changes in discharge, channel width, resistance, roughness, sediment load, and sediment caliber. Finally, we consider how incision processes, such as plucking, that are independent of bed load might influence the development of a hanging valley. We suggest that the rapid pace of climate change and corresponding variability in sediment discharge and caliber commonly promote pulses of aggradation that precipitate the destruction of incipient hanging valleys.

2. Prediction of Erosion Rates

[5] When bed load moves downstream by saltation, each impact may remove a small amount of bedrock if overlying sediment does not cushion the force. Considerable progress has already been made in describing this process. Sklar and Dietrich [2004] synthesized many empirical relationships to develop an equation predicting the rate of erosion (E) that saltating bed load causes in bedrock channels whereby:

$$E = \left[\frac{0.08 R_b g Y}{k_r \sigma_T^2} \right] \left[Q_s \left(\frac{\tau^*}{\tau_c^*} - 1 \right)^{-\frac{1}{2}} \right] \left(1 - \frac{Q_s}{Q_t} \right) \left[\left(1 - \left(\frac{u^*}{w_f} \right)^2 \right)^{\frac{3}{2}} \right]. \quad (1)$$

The first term describes how much bedrock can be removed by a particle impact. This depends on the non-dimensional buoyant density (R_b) of the sediment, gravitational acceleration (g), and physical properties of the bedrock underlying

the channel: elastic modulus (Y), resistance parameter (k_v), and tensile strength (σ_T). The next term describes the effect of the bed load sediment supply (Q_s). This is modulated by the nondimensional shear stress, or Shields stress (τ^* : equation (2)), in excess of the Shields stress at the threshold of particle motion (τ_c^*).

$$\tau^* = \frac{R_h S}{R_b D_s}. \quad (2)$$

D_s is the diameter of impacting particles, and the hydraulic radius [$R_h = HW/(2H+W)$] is found by numerically solving the Manning equation:

$$Q = HW \left(\frac{R_h^2 S^2}{n} \right), \quad (3)$$

where Q is the water discharge in the channel, H is the flow depth, W is the width, S is the slope, and n is Manning's roughness. The third term in equation (1) describes the decrease in erosion rate as sediment supply approaches transport capacity (Q_t) [Fernandez-Luque and van Beek, 1976],

$$Q_t = 5.7 \rho_s W \sqrt{R_b g D_s^3} (\tau^* - \tau_c^*)^{3/2} \quad (4)$$

and the bed becomes protected from impacts. The final term in equation (1) describes the decrease in erosion rate as bed load particles enter suspension. This transition occurs as the shear velocity (u^*) surpasses the particle settling velocity (w_p) calculated using the Dietrich [1982] empirical formula. Numerical attempts to predict the shape of river long profiles with this model have been only partly successful [Gasparini et al., 2007; Sklar and Dietrich, 1998; Tomkin et al., 2003; Whipple and Tucker, 2002]. One source of difficulty is that, as predicted by this equation, small streams with steep slopes and limited bed load supplies tend to have a limited capability to erode. Instead of steep slopes always leading to increased erosion, this description of channel erosion predicts that bed load particles will impact the bed less frequently and remove less material when channel slope increases beyond a critical value.

[6] Others have argued that the limited erosional capability of small streams with steep slopes explains the formation of hanging fluvial valleys where small tributaries enter much larger, rapidly incising trunk streams [Crosby and Whipple, 2006; Crosby et al., 2007; Wobus et al., 2006]. Whereas naturally occurring hanging fluvial valleys are observed under such conditions, they are not ubiquitous even in regions where the presence of some hanging fluvial valleys suggests that incision via bed load saltation is a dominant process.

3. Model Setup

[7] We model three linked channel reaches (upper trunk, tributary, and lower trunk) that experience a steady drop in local base level. The bed load saltation model (equation (1)) predicts the channel slope needed to drive incision at a rate

Table 1. Default Modeling Parameters for a 500 km² Drainage^a

Parameter	Value
Channel slope	
Lower trunk	0.00178
Upper trunk	0.00183
Tributary	0.00381
Discharge (lower trunk)	350 m ³ /s
Clast diameter ^b	0.060 m
Sediment supply (lower trunk)	125 kg/s
Manning's roughness ^b	0.035
Rock tensile strength ^b	7.0 MPa
Rock Young's modulus ^b	5·10 ⁴ MPa
Frequency of bed load movement	10 d/a
Channel width	
Lower trunk	31 m
Upper trunk	30 m
Tributary	14 m
Rock density ^b	2650 kg/m ³
Water density ^b	1000 kg/m ³
Water kinematic viscosity	1·10 ⁻⁶ m ² /s
Trunk to tributary area ratio	1:10
Critical shear stress ^b	0.030
Rock resistance parameter ^b	1.0·10 ¹²
Powers roundness ^b	3.5
Corey shape factor ^b	0.8

^aThese values describe the tributary junction at equilibrium with 0.5 mm/a of base-level fall. The channel may adjust to changes in base level and climate through adjustments in slope. Clast diameter, discharge, frequency of bed load movement, and sediment supply, may be varied to simulate climate change.

^bAssumed following Sklar and Dietrich [2004].

equal to the rate of base-level fall in both the trunk and tributary. The parameters used in this steady state profile are included in Table 1. We then perturb the resultant steady state tributary via changes in the rate of base-level fall and climate-controlled parameters.

[8] Our application of the Sklar and Dietrich [2004] model utilizes many of the simplifications used by Snow and Slingerland [1990] in their numerical model of rejuvenated fluvial networks. Our model assumes a straight channel with a rectangular cross-section and a fixed width. We only consider a 2-km-long channel reach on the main stem and a 1-km-long reach on the tributary. Above and below their confluence, discharge is held constant, such that adjusted channel slopes are uniform. Changes in the rate of base-level fall are applied at the downstream end of the modeled trunk stream, as if controlled by steady fault offset. A single clast size and shape are assumed to approximate the average effect of the range of clasts in a natural stream. Similarly, a reference discharge and reference sediment supply approximate the effects of a wide range of discharges and sediment supplies (Table 1). We also assume a uniform rock type in both channel bed and bed load material. Additionally, we assume that eroded bedrock does not contribute to the supply of bed load downstream. In our modeling, all erosion is assumed to occur during a few, high-flow events per year.

[9] Following the strategy of other researchers [Hancock and Anderson, 2002; Snow and Slingerland, 1987, 1990], the stream channel is modeled as a series of cells. All of the model parameters are the same within a single 20-m-long cell, but may differ between cells. Unlike in Hancock and Anderson's [2002] approach, only vertical incision is considered, and the more complicated formula for erosion rate provided by Sklar and Dietrich [2004] is used. Explicitly

modeling the deposition of fill in channel cells where the sediment load exceeds the transport capacity would require much shorter time steps than the erosion of bedrock requires. Instead, wherever the bed load supply exceeds transport capacity, fill is added on top of the bedrock channel to achieve the required transport slope. No bedrock erosion may occur in channel cells covered by fill.

4. Selection of Model Parameters

[10] Five years of suspended sediment load and discharge measurements from the Khudi River, a tributary of the Marsyandi River in central Nepal (Figure 1) [Gabet *et al.*, 2008], guide the selection of a reasonable combination of bed load sediment supply and discharge. Like the drainages where Wobus *et al.* [2006] observed hanging fluvial valleys in Taiwan, the Khudi catchment receives heavy precipitation during the annual monsoon (~ 4 m/monsoon [Burbank *et al.*, 2003]). Assuming that (1) bed load is mobilized when the suspended load is greatest, (2) bed load mobilization occurs on an average of 10 d/a, and (3) the bed load flux is one half the suspended load flux during these times of mobilization [Pratt-Sitaula *et al.*, 2007], an estimate of the bed load flux can be made. Finally, these estimates are scaled up from the 136-km² drainage of the Khudi to the 500-km²-model drainage area (Table 1). This drainage size is chosen to be similar to the trunk drainage areas in northeastern Taiwan [Wobus *et al.*, 2006].

[11] The tributary is modeled as a stream whose drainage basin area is 10% of the total area drained by the trunk stream. Assuming that discharge and sediment load are proportional to drainage area, the tributary contributes 10% of the discharge and sediment load of the trunk stream. These values are chosen on the basis of the observations by Wobus *et al.* [2006] that, in Taiwan, hanging valleys tend to form where the ratio of tributary to trunk area is 1:10 or less. In our initial model, the lowering rate at the downstream end of the trunk channel is 0.5 mm/a, the bed load flux in the lower trunk when mobilized is 125 kg/s, and the discharge is 350 m³/s.

[12] Channel width of each section of stream in the model is estimated using the power law:

$$W = kA^\omega \quad (5)$$

where A is the drainage area and k and ω are empirical constants. The average values of $k = 3.3$ and $\omega = 0.36$ based on the compilation of bedrock river data by Whipple [2004] are used.

5. Numerical Experiments

5.1. Slow Base-Level Fall and Channel Incision

[13] In the initial condition, the slopes of the main and tributary rivers are fully adjusted such that the rate of channel erosion exactly and ubiquitously balances the 0.5 mm/a rate of base-level fall. If the rate of base-level fall abruptly increases to 0.7 mm/a, both the trunk and tributary eventually become steeper and are able to incise as rapidly as base-level falls (Figure 2). The change in channel slope required to incise at 0.7 mm/a is small so the boundary between the adjusted, steeper reach and the unadjusted reaches is repre-

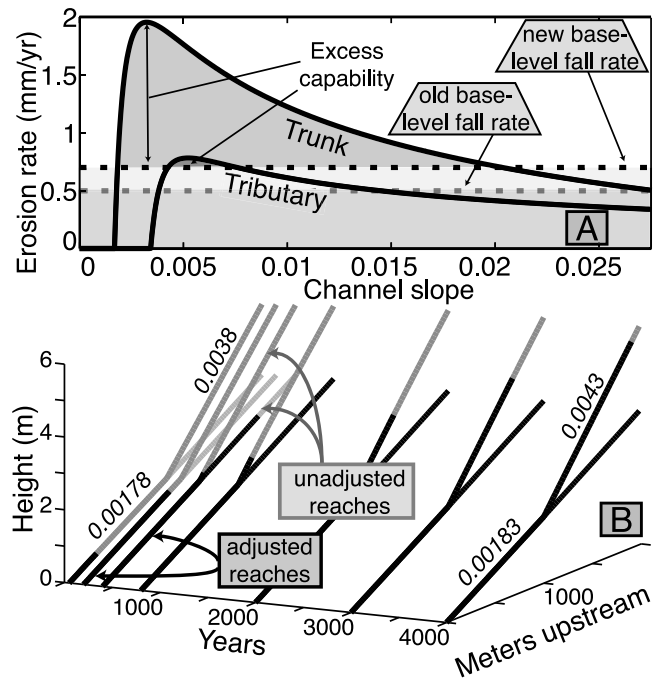


Figure 2. Tributary junction response to increased rate of base-level fall from 0.5 mm/a to 0.7 mm/a. (a) Predicted erosion rates in the modeled trunk and tributary reaches over a range of channel slope. Where these curves intersect the dashed lines representing base-level fall rate, erosion and base-level fall are balanced. Both trunk and tributary have excess erosional capability. (b) Profiles of a 2-km-long channel reach with a tributary joining at the midpoint show the adjustment to an increased rate of base-level fall through time. The change in rate of base-level fall is imposed at the bottom (0 m) of the modeled reach. The black reaches of the profiles are adjusted to base-level fall at 0.7 mm/a and are slightly steeper. Channel slopes for adjusted and unadjusted reaches are indicated in italics.

sented by a subtle convexity. After 4,000 model years, the knickpoint has nearly migrated past the upstream limit of the modeled channels; they are fully adjusted.

5.2. Rapid Base-Level Fall and Formation of Hanging Valleys

[14] When the rate of base-level fall is increased from 0.5 mm/a to 1 mm/a (Figure 3), the tributary is incapable of incising at this rate, and a hanging valley begins to develop at the tributary mouth in a style analogous to the modeling by Crosby *et al.* [2007]. As the knickpoint on the trunk stream passes the tributary junction, the tributary mouth steepens. Initially, the steeper tributary mouth allows enhanced incision, and a knickpoint begins to migrate up the trunk stream. The slope at the tributary mouth, however, continues to become steeper because the tributary is unable to incise as quickly as the trunk stream. Once the tributary mouth slope exceeds a critical value (about 0.005, given the specified parameters such as Q , Q_s , and clast size), the rate of incision at the tributary mouth begins to decline with increasing channel slope. When the tributary mouth has steepened beyond its maximum capability to incise, the tributary is

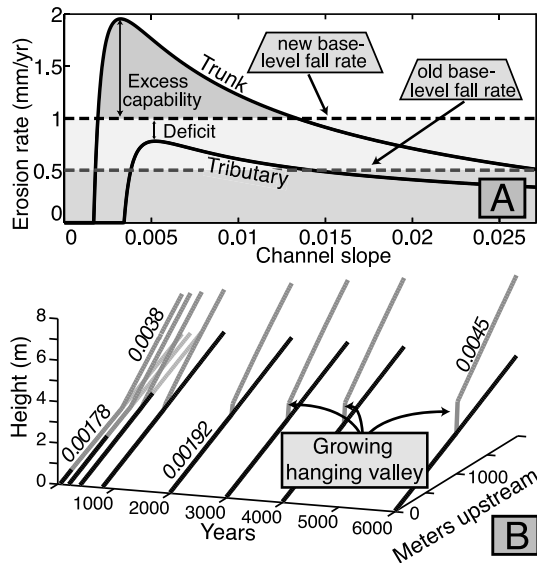


Figure 3. Tributary junction response to increased rate of base-level fall from 0.5 mm/a to 1 mm/a. (a) Curves show predicted erosion rates in the modeled trunk and tributary reaches over a range of channel slope. The rate of base-level fall exceeds the tributary capability to erode because increased channel slope cannot cause incision at 1 mm/a. (b) Because the tributary cannot incise as quickly as the trunk, an incipient hanging valley forms at the tributary mouth. Only the trunk stream profile adjusts to the change in base-level fall. The adjusted channel reaches are shown in black, and the unadjusted reaches are shown in gray. Channel slopes are indicated in italics. This nascent hanging valley which was developed through 6,000 model years is used in subsequent models to demonstrate the degradation of hanging valleys.

essentially isolated from downstream changes in base level. The trunk stream continues to incise at 1 mm/a, but the tributary incision rate decreases, and the steepened reach at its mouth continues to grow in height.

6. Climate-Controlled Parameters

[15] Whereas hanging fluvial valleys are evident in some tectonic terrains [Crosby and Whipple, 2006; Wobus *et al.*, 2006], they are uncommon, even in rapidly eroding landscapes. On the other hand, our model predicts that, wherever a trunk stream persistently incises more quickly than one of its tributaries, a hanging fluvial valley will form, and its height will progressively grow. For the example above, the hanging valley reach would gain nearly 1 m in height every 1 ka, as long as the controlling parameters remain constant. Given such predictions, why are hanging valleys not more common? One possibility is that, because this model only considers one erosional process (bed load saltation), it may underpredict total erosional capabilities of a stream. For most other numerical models of channel erosion, the rate of erosion is predicted to increase as the channel slope steepens [Crosby *et al.*, 2007; Lamb *et al.*, 2008]. Hence, in reality, the contributions of other processes, such as wear by suspended load, cavitation, and plucking, might allow many streams to incise more rapidly than our model predicts, such that a

hanging valley might not form at all. A second possibility that is more relevant to Marsyandi tributaries (Figure 1), where the presence of numerous hanging valleys suggests the dominance of bed load–dependent incision, is that changes in climate might alter some of the parameters of the bed load–saltation process [Sklar and Dietrich, 2004] and cause hanging valleys to disappear or diminish. We explore this second hypothesis by examining the impact on incision rates resulting from changes in discharge, sediment load, and frequency of bed load mobilization. The following numerical experiments predict those conditions under which a hanging valley would be more likely to degrade: increased bed load or increased flood frequency, but not increased discharge.

6.1. Increased Discharge

[16] If the discharge in both the tributary and the trunk increases, these changes alone are insufficient to cause the incipient hanging valley to degrade. No change occurs in the predicted peak erosion rate; instead, the channel slope at which peak erosion is attained lessens (Figure 4a). The increase in discharge increases Shields stress (equation (2)) in all reaches of the modeled streams, but the effect of these changes diverges between the trunk and tributary. The trunk stream is no longer in equilibrium with the rate of base-level fall and is (initially) slightly oversteepened in this new climatic regime. It therefore responds by becoming gentler. In contrast, at the tributary mouth, increased Shields stress drives bed load particles to take longer hops and leads to a further decrease in the rate of bed load impacts and erosion. In this example, the hanging valley continues to grow in height as the trunk incises more quickly than the tributary.

6.2. Increased Flood Frequency

[17] In the context of increasing storminess, we consider a doubled frequency of bed load mobilizing events (Figures 4b and 4c). Recall that only the tributary mouth is steepened beyond its maximum erosional capability. The rest of the tributary reach has a gentler slope and is isolated from base-level adjustments in the trunk stream. This change in model parameters allows the tributary to incise at up to 1.5 mm/a and the trunk to incise at nearly 4 mm/a because erosional events are more frequent (Figure 4b). As a consequence, both the trunk and tributary are predicted to incise more quickly than base-level falls. The trunk stream adjusts by establishing a gentler gradient that allows it to incise at only 1 mm/a, thereby balancing the rate of base-level fall.

[18] Initially, the incipient hanging valley grows higher and steeper instead of diminishing because the unadjusted trunk reach still incises more quickly than the tributary (Figure 4c). Once the adjusted and now gentler trunk reach extends past the tributary mouth, the tributary incision rate exceeds that of the trunk, and the hanging valley begins to diminish in height. The hanging valley degrades from the top down. Once this happens, the tributary also establishes a gentler gradient that allows it to incise at the same rate as the trunk.

[19] Doubling the frequency of flood events served to double the capabilities of the streams to incise, and the tributary slope inherited from the unperturbed climate regime was steep enough to drive incision faster than the base-level lowering rate. The tributary only incises as fast as the inherited

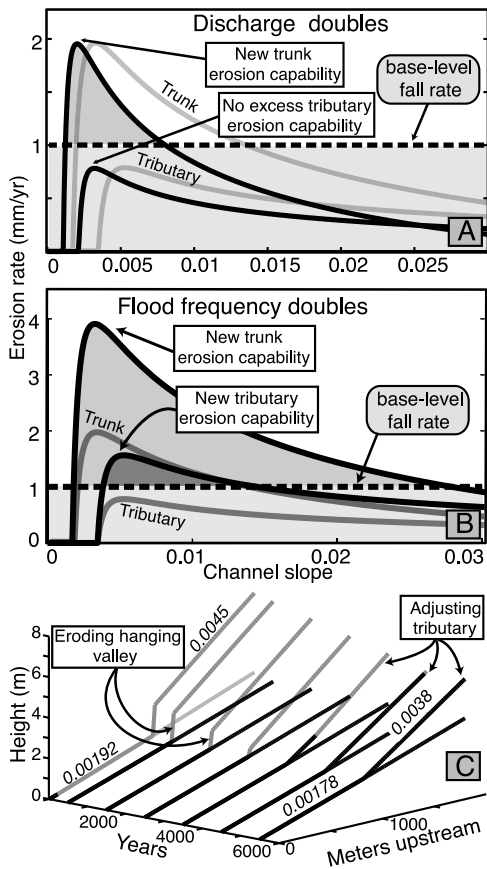


Figure 4. Tributary response to two climate change scenarios. (a) Doubling discharge decreases the slope required to drive erosion at a given rate. The black curves are shifted left relative to the gray curves that represent erosional capability without climatic perturbation. Doubled discharge does not provide the tributary with excess erosional capability. (b) Climate change modeled as doubling the frequency of bed load mobilization increases the erosional capability of both the trunk and tributary (black curves). Tributary erosional capability now exceeds the uplift rate (dashed line). (c) The initial channel profile represents the tributary junction with a stationary knickpoint formed after 6,000 years of trunk incision in Figure 3. Doubling the frequency of bed load mobilization causes the knickpoint to degrade and reestablishes a concordant tributary junction. Adjusted channel reaches are shown in black, and channel slopes are indicated in italics.

channel slope allows unless the change in parameters reconnects the tributary with the trunk base-level signal via channel aggradation.

6.3. Double Discharge and Increase Bed Load Supply Tenfold

[20] In this numerical experiment, the frequency of bed load mobilization remains 10 d/a, but the size of these events increases such that sediment supply overwhelms the trunk transport capacity. The widespread occurrence of fill terraces in mountain river valleys attests to the time-varying ability of channels to transport the sediment supplied to them. The most common cause of such variability in sediment loads

appears to be climate change [Bookhagen et al., 2005a; Hancock and Anderson, 2002; Pan et al., 2003]. Aggradation can also be driven by seismically triggered landslides [Harp and Jibson, 1996], either by damming valleys and trapping sediment [Ouimet et al., 2007; Pratt-Sitaula et al., 2007] or by an increased hillslope-derived sediment flux [Dadson et al., 2004].

[21] Following the formulation by Hancock and Anderson [2002] in their efforts to model the formation of river terraces in response to climate change, we model a doubling of discharge and a tenfold increase in the sediment supply. These changes permit the tributary channel to erode at ~3 mm/a at a slope of ~0.01 (Figure 5). We recognize that a tenfold increase in the bed load flux probably represents an upper limit of likely changes. On the other hand, several factors suggest that multifold bed load increases should be expected. For example, whereas the sediment load in our reference model is based on 5 years of suspended sediment measurements [Gabet et al., 2008], reconstructed erosion rates for the past few hundred years deduced from detrital cosmogenic nuclide concentrations for the same catchment [Niemi et al., 2005] are about twice as large as the current rates and are more consistent with long-term erosion rates based on numerous bedrock fission-track ages in this area [Whipp et al., 2007]. Moreover, compared to the late Holocene, sediment fluxes from the Himalaya approximately doubled during the early Holocene [Goodbred and Kuehl, 1999] when the monsoon was stronger. Finally, we suspect that higher, early Holocene sediment fluxes were at least in part due to higher rates of landsliding [e.g., Bookhagen et al., 2005a]. If so, we expect the fraction of coarse sediment in the total sediment flux to increase [Attal and Lavé, 2006]. With respect to our reference model, the summation of these factors could increase the bed load flux at least fivefold and perhaps considerably more.

[22] In this simulation, the increased bed load supply exceeds the trunk transport capacity, such that a wedge of sediment establishes a gradient steep enough to transport the sediment load (Figure 6). The thickness of fill increases upstream and buries the hanging fluvial valley. The tributary, which had been isolated from the base-level signal by the

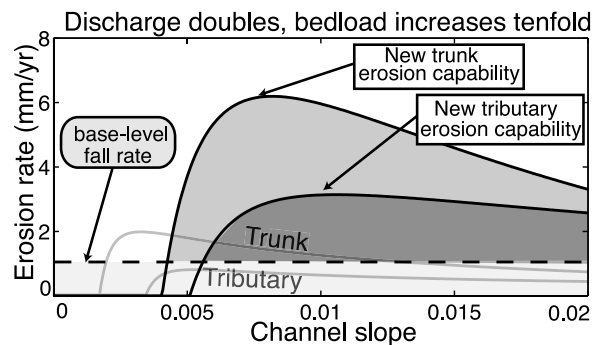
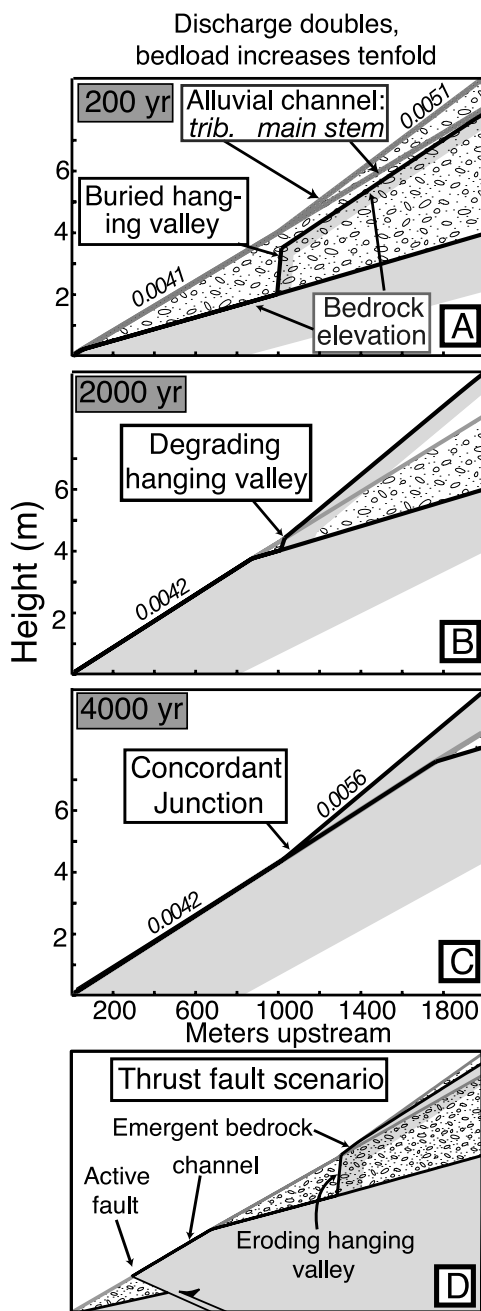


Figure 5. Climate change marked by a doubled discharge during bed load mobilization and a tenfold increase in bed load supply greatly increases trunk and tributary erosional capability (black curves). This enhanced capability exceeds the rate of base-level fall (dashed line), and the bed load supply exceeds the transport capacity of the trunk and tributary at their previous gradients.

hanging valley, now reconnects to it via the alluviated channel surface. This alluvial fill prevents the streams from incising the underlying bedrock channels. A knickpoint forms at the base of the trunk stream where steady base-level fall steepens the channel enough for fill to be removed and for bedrock incision at 1 mm/a to resume, thereby keeping pace with the rate of base-level fall. It is perhaps more intuitive to envision changing base level, in this case, as being due to differential rock uplift along a thrust fault that causes the bedrock surface to approach and then emerge through the alluvial surface (Figure 6d). The knickpoint that then forms represents a subtle increase in channel slope from 0.0041 (alluvial) to 0.0042 (bedrock) that migrates upstream. As the knickpoint in the trunk channel migrates, the thickness of fill begins to thin upstream, and eventually, the bedrock crest of the hanging valley reach is exposed above the tributary

mouth. The added erosional tools provided by the increased sediment load cause the tributary mouth to incise its bedrock channel as quickly as the trunk stream lowers its alluviated bed (Figure 6b). Because the tributary mouth had been elevated above the trunk stream, bedrock incision in the tributary channel, especially of the lip of the hanging bedrock valley, resumes before all fill is removed from the trunk stream. Persistent bedrock erosion gradually lowers the hanging valley and allows the tributary channel to reestablish concordance with the trunk bedrock channel (Figure 6c).

[23] The modeled hanging valley could still degrade even if bed load sediment supply did not increase as dramatically as in this example. For this to occur, three conditions would have to be met. The enhanced sediment supply should exceed the trunk stream transport capacity thereby causing aggradation. Sufficient tools must be available for the tributary to erode as rapidly as the rate of fall in base level (Figure 7). Finally, the wedge of sediment that is required to establish the transport gradient in the trunk should begin far enough downstream of the tributary junction that its thickness buries the hanging valley and reconnects the tributary with the trunk base level. In our example with the tributary junction situated only 1 km upstream of the base-level control point, a trunk stream transport slope of 0.004 is required to bury the hanging valley. Given that channel aggradation could begin farther down stream of natural tributary junctions, a wide combination of trunk slope, discharge, and bed load conditions would allow the tributary hanging valley to initially be buried and then to degrade (Figure 7).



7. Maximum Erosional Capability

[24] In order for any adjustment of model parameters to allow for hanging valleys to degrade, the tributary maximum capability to incise must increase above the rate of base-level fall. When tributary erosion rates are calculated as a function of channel slope (Figures 2a, 3a, 4a, 4b, and 5), the maximum possible erosion rate in each simulation represents the highest rate of incision that the stream is capable of producing through changes in channel gradient. The effect of different

Figure 6. Channel elevation profiles show the effects over time of doubling discharge and increasing bed load supply by a factor of 10. Channel slope and transport slope values are indicated in italics. (a) After 200 years, enhanced bed load supply overwhelms transport capacity, causing channel aggradation. Bedrock-floored channel reaches are shown in black. The difference between channel elevation (gray reaches) and bedrock elevation represents the thickness of fill (stippled pattern) required to create channel slopes steep enough to transport the enhanced sediment load. (b) After 2000 years, base-level fall continues at 1 mm/a and a bedrock channel is reestablished. The buried hanging valley degrades as bedrock is exposed in the tributary. (c) After 4000 years, a concordant junction is established with channel gradients adjusted to erode at 1 mm/a and transport the large sediment load. (d) This diagrammatic representation of base-level fall driven by a thrust fault illustrates that the controls on fill depth at the hanging valley are transport slope, bedrock channel slope, and the downstream extent of the alluviated surface.

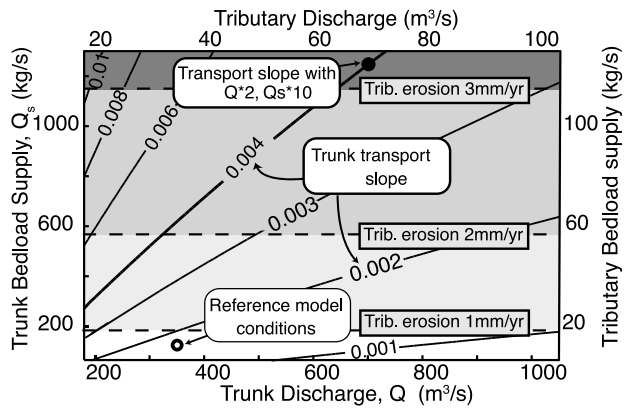


Figure 7. Interplay between bed load supply and discharge in affecting trunk transport slope and the effect of equivalent changes in the tributary on its erosional capability. The bottom and left axes represent parameters in the trunk stream. The top and right axes represent equivalent values in a tributary that is one-tenth the size. The tenfold increase in sediment load with a doubling of discharge can only be transported on a slope greater than 0.004 (solid dot). These new parameters allow the tributary to incise at over 3 mm/a with sufficient steepening. The same transport slope, and depth of channel aggradation, could be achieved with any combination of trunk discharge and sediment load that plots along this line of equal transport slope. So long as the supply of bed load in the tributary allows incision at greater than 1 mm/a, the incipient hanging valley will degrade as in Figure 6. Gentler transport slopes also cause hanging valley burial and removal if the tributary junction is farther upstream from the base-level control point and the coincident beginning of the alluviated reach.

parameters on this erosive capability is demonstrated by plotting this maximum value (found through numerical optimization) as a function of a varying stream parameter (Figure 8).

[25] The tributary slope required to initiate hanging valley formation in the reference model (Figure 3) is lower than the slopes observed in Marsyandi tributaries. This mismatch suggests that the reference model parameters do not adequately describe the Marsyandi system. Given the highly simplified model, such a discrepancy is not unexpected. The following analysis of model sensitivity indicates which parameters could influence the tributary slope at which hanging valleys form. Note that in this exploration of parameter space, only one variable is changed at a time, which is a situation that may be uncommon or even untenable in nature, given likely interactions among variables. Nonetheless, this exploration provides insight on the role played by specific variables and leads to some intuitive, as well as some unexpected, results.

[26] As drainage area increases (Figure 8a), the supply of bed load tools grows more quickly than the channel widens. Larger tributaries have more bed load per unit of channel width than smaller tributaries and are capable of incising more quickly. On the other hand, tributary erosional capability is insensitive to changes in discharge (Figure 8b) and roughness (Figure 8c), because these do not affect the supply

of impacting bed load clasts. They do, however, increase the Shields stress and cause peak incision rates at lower tributary slopes.

[27] Decreasing channel width concentrates bed load tools across a smaller area and enhances the tributary erosional capability (Figure 8d). Thus, if channels narrow in response to steepening [Finnegan *et al.*, 2005; Cowie *et al.*, 2006], erosional capability would increase and hanging valleys would be less likely to form. As a function of channel width, the slope required to drive maximum erosion has a local minimum. Slope is minimized when the wetted perimeter of the tributary is also at a minimum.

[28] The modeled tributary would be able to incise more quickly if the clast size increased, despite the same total mass of bed load moving through it (Figure 8e), or if that load moved during smaller, more frequent events (Figure 8f). As expected, the maximum erosion rate is highly sensitive to both rock resistance (Figure 8g) and the tributary bed load (Figure 8h). As long as the tributary channel slope is free to adjust to be steep enough to transport the bed load, effective shielding of the bed and decreases in erosion rates only occur at extreme transport rates: greater than 1200 kg/s (Figure 8h).

[29] This examination of how the maximum capability to erode varies with model parameters suggests that some climatically sensitive parameters, such as flood frequency, bed load, or clast size, could have a major impact on tributary erosion rates and would, therefore, influence the formation or degradation of hanging fluvial valleys. Notably, many of the assumptions used to develop this model, such as fixed channel width, are not likely to provide an accurate description of natural drainages. Depending on how these simplifying assumptions were varied within the numerical model, they could either promote or inhibit the formation of hanging valleys (Figure 8).

8. Bed Load Saltation and Plucking

[30] Thus far, our numerical simulations have only modeled erosion by a single process: that of bed load impacts. Indeed, Crosby *et al.*'s [2007] modeling suggests that, of the common fluvial erosion models, only saltation models lead to hanging valley creation. One consequence of employing only saltation erosion is that hanging valleys are readily formed in zones of rapid base-level lowering. Furthermore, in a bed load-impact-only model, once a stationary knickpoint forms at a tributary junction, it can only become higher and steeper, but it does not extend farther upstream. In our results thus far, the length of the over-steepened reach is as short as the model grid spacing. Except where hanging valleys in nature are represented by waterfalls, however, they are rarely so limited in spatial extent. Modeling the effects of another erosional process in concert with bed load impacts can produce more reasonable longitudinal profiles when higher uplift rates or longer periods of hanging valley growth are modeled.

[31] Abrasion by suspended loads [Lamb *et al.*, 2008] and plucking of bedrock particles from the channel [Snyder *et al.*, 2003] can occur on channel reaches where shear stress is elevated. Particle impacts may not be required for plucking to occur, so that on very steep bedrock channel reaches, erosion may still occur where impacts from descending particles are infrequent or ineffective. We, therefore, incorporate into our bed load-saltation model, a model for channel incision based

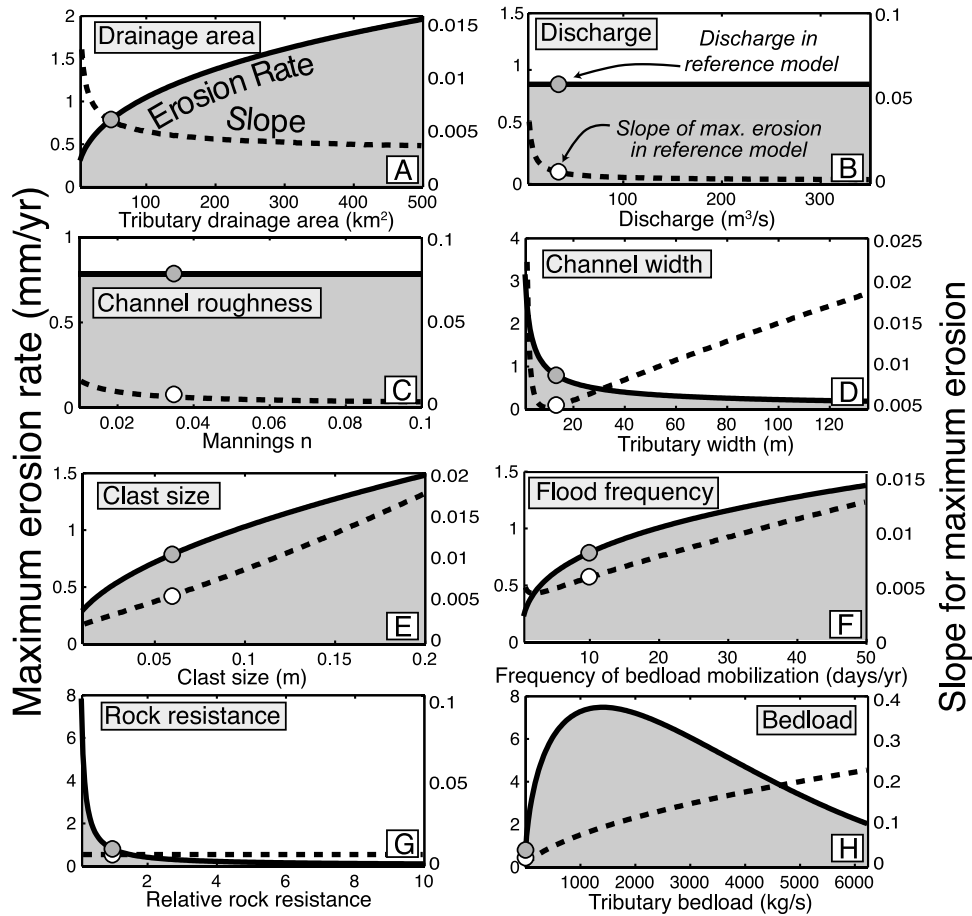


Figure 8. Peak tributary erosional capability is plotted as a function of eight saltation-abrasion model parameters (black curves). The channel gradient required to drive maximum erosion is shown as a dashed line. The filled circles indicate the peak erosional capability of the tributary stream in the reference model without climatic perturbation, and the open circles represent the tributary slope that drives peak erosion in this reference model (see Table 1 for parameters).

on shear stress in excess of an erosion threshold that has been calibrated for several drainages in the Himalaya [Lavé and Avouac, 2001].

$$E_P = K_P(\tau^* - \tau_P^*), \quad (6)$$

which relates the Shields stress (τ^*) in excess of that required to remove bedrock particles of a given size to the erosion rate caused by plucking (E_P) with a proportionality constant (K_P). The value τ_P^* refers to the Shields stress required to initiate plucking. We choose $\tau_P^* = 0.06$, twice the threshold for the initiation of bed load movement and assume that plucked particles are 0.5 cm in diameter. Lavé and Avouac [2001] calibrated the proportionality constant to Himalayan rock types and found that $K_P \approx 8$ mm/a best described the sensitivity of incision to Shields stress in the Lesser Himalaya. Summing equations (1) and (6) yields an erosion formula describing both erosion through bed load impacts and erosion through some process like plucking.

[32] The model results suggest that, when Shields stress is very low, neither the threshold for bed load movement nor the threshold for bedrock plucking are met so both E (from equation (1) [Sklar and Dietrich, 2004]) and E_P are 0. If

Shields stress is greater than τ_c^* , but less than τ_P^* , erosion only occurs through bed load saltation. If Shields stress increases to the point that bed load saltation is ineffective, while the stress simultaneously exceeds the threshold for plucking, erosion through plucking will dominate.

[33] In order to demonstrate this extended erosion equation, we simulate base-level fall at a rate of 4 mm/a with bed load supply increased sixfold. Unlike previous examples (e.g., Figure 3), steep channel reaches develop in this scenario. Therefore, Shields stress is calculated using the sine of the slope angle (α) rather than the small angle approximation, $S \approx \sin(\alpha)$. In the present scenario after 80,000 model years, the hanging valley has steepened enough (channel slope > 0.6 ; Figure 9b) for plucking to drive incision at 4 mm/a (Figure 9a) and, hence, to balance the rate of trunk stream lowering. Prior to achieving this slope, plucking erodes the tributary at less than the rate of main stem erosion (Figure 9a), such that the height of the hanging valley continues to grow. Erosion by plucking allows the crest of the steepened reach to migrate upstream, thereby progressively replacing the gentle upstream slope with a steep one (see profiles T_1 and T_2 , Figure 9b). If the simulation were to run for many more thousands of years, the entire modeled tributary reach could

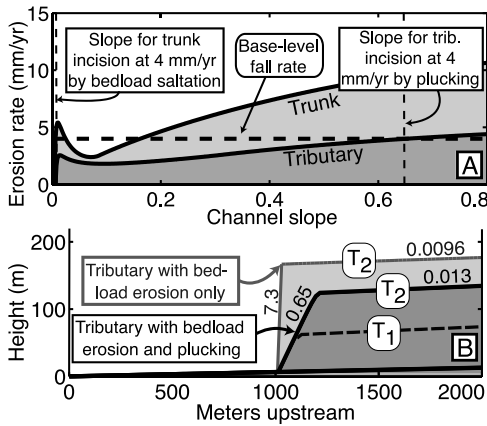


Figure 9. Model in which tributary mouth incises via plucking on the steep reach where bed load saltation is ineffective. (a) Black curves show response to steepening of the trunk and tributary erosion rate for a combined bed load and plucking model. (b) Black channel profiles show that after 80 ka (T_2) a reach several 100 m long at the tributary mouth is steep enough to incise via plucking. Though the tributary upstream of the hanging valley is still unable to incise as quickly as the trunk stream, it incises its bed more quickly than the same scenario when only bed load incision is modeled (gray profiles). Channel slopes are indicated in italics. An intermediate stage of hanging valley growth with plucking is also shown (T_1).

become steep enough to incise via plucking at 4 mm/a. Until that time, however, the gentle tributary channel above the steepened reach erodes more slowly than the trunk stream, causing increased relief between the tributary and trunk streams. Factors that affect the Shields stress, τ^* (equation (2)), such as increasing discharge, decreasing channel width, and decreasing the size of bed load particles plucked from the channel bed, would allow the tributary mouth to incise at the same rate with diminished channel gradient.

[34] Using this simple description of how a bed load-independent erosion process may act on steep channel slopes in concert with bed load saltation erosion, we have not attempted to capture the behavior of saltating bed load on steep channel slopes. For example, the *Sklar and Dietrich* [2004] equation assumes that as bed load strikes the channel bed, its descent velocity approximates its velocity component perpendicular to the bed. On steeper slopes, however, the descent velocity is no longer nearly perpendicular to the bed. Given that this equation was developed to describe the erosional effects of bed load on gently sloping channel beds, it may not capture some features of bed load-dependent erosion on steeper slopes.

9. Discussion

[35] “Playfair’s Law” of accordant stream junctions [*Playfair*, 1802] is violated by the presence of hanging valleys with steepened reaches as much as 1 km in height in Taiwan and Nepal. A bed load-dependent incision rule implies that hanging valleys should readily form wherever small tributaries enter rapidly incising trunk streams and are unable to incise their beds as rapidly as the trunk channel.

[36] A key factor limiting the formation of hanging tributaries is the rate of base-level fall. Numerical simulations of this single erosional process predict that hanging fluvial valleys only form at tributary mouths when the rate of trunk stream incision exceeds the maximum possible rate of tributary incision (Figure 3). Some, but not all, variations in climate-controlled variables can increase this erosional capacity above the rate of base-level fall and either inhibit the formation of hanging valleys or cause them to degrade (Figure 10). In particular, increases in bed load supply and caliber and decreases in channel width promote degradation of existing hanging valleys, whereas increases in discharge and channel roughness do not change maximum erosion rate, but change the slope at which maximum erosion is predicted to occur.

[37] Many of the assumptions used in the numerical simulations of hanging tributary junctions could mask natural variability among tributaries and between a tributary and trunk stream that could inhibit or promote the formation of hanging fluvial valleys. For example, our modeled tributary does not narrow in response to base-level fall even though such an adjustment might have allowed it to incise as quickly as the trunk stream [*Amos and Burbank*, 2007; *Whittaker et al.*, 2007]. Bed load supply could also differ between a small tributary and larger trunk stream. The mass flux of bed load in smaller tributary drainages may be coarser and make up a larger fraction of the total sediment load [*Sklar et al.*, 2006]. If so, our initial assumption that bed load supply was proportional to drainage area in both the trunk and tributary and that bed load caliber did not vary between them would be violated. Modest increases in tributary bed load flux (Figure 8h) or flood frequency (Figure 8f) would enhance erosional capacity in the tributary. If bed load caliber were also greater (Figure 8e), erosional capacity could further increase in the modeled tributary and retard the formation of hanging valleys.

[38] Changing climate-controlled parameters can also increase the bed load supply beyond the trunk transport capacity (equation (4)) causing bedrock channels to aggrade. Sedimentary fill may bury a hanging valley and reestablish a concordant tributary junction in alluvial sediment (Figure 6).

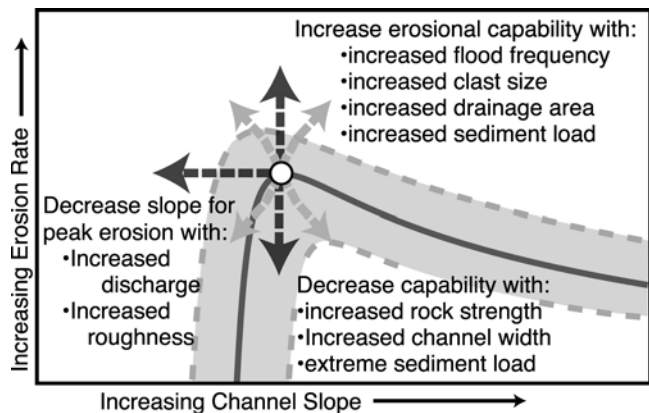


Figure 10. Summary of erosional capability dependence illustrating those factors that can enhance or suppress bed load erosion capability and those to which it is insensitive. Many of the factors listed as affecting peak erosion rate also affect the channel slope required for peak erosion.

Not only will the steepened bedrock reach be invisible below the channel surface, but as fill degrades, the hanging valley may be eroded away if sufficient bed load tools are available in the tributary.

[39] We speculate that the high probability of variations of sediment supply due to past climatic changes explains why hanging tributary valleys are uncommon, even in many moderately active orogens. As long as the magnitude of climatically driven aggradation exceeds the height of a steep tributary knickpoint formed since the last aggradational event, our models predict that any nascent hanging valley would be buried and then degraded in the tributary.

[40] Although reliable reconstructions of variability of past riverine sediment fluxes are typically unavailable at climatic time scales ($\sim 10^3 - 10^4$ years), documented episodes of rapid aggradation of alluvial fills (10–25 mm/a [e.g., Bull, 1991; Bookhagen et al., 2006]) attest to abrupt swings in sediment supply relative to transport capacity and reveal aggradational rates that far outpace tectonic rates of differential uplift or subsidence. Doubling of sediment fluxes in the Himalaya during the intensified early Holocene monsoon [Goodbred and Kuehl, 1999] and synchronous deep aggradation within steep river valleys [Bookhagen et al., 2005b, Pratt et al., 2002] suggests that 10s to 100s of meters of aggradation in mountain valleys can occur within a few millennia when sediment fluxes increase. If steepened reaches existed at the mouths of hanging tributaries at such times, aggradational events of this magnitude would be expected to bury many of them. Our modeling suggests that the subsequent degradation of this fill would be likely to destroy previously formed hanging valleys in the underlying bedrock channels.

[41] If we were to posit climatically driven events of sediment aggradation every 20 ka (for example, by mimicking the frequency of precessional cycles [Clemens and Prell, 2003]), then for any base-level lowering rate of 0.5 mm/a or less, our model predicts that as little as 10 m of aggradation would bury an incipient hanging valley and lead to its destruction. Aggradational events of this magnitude appear common in most mountain ranges. We hypothesize, therefore, that the presence of hanging valleys in the Nepalese Himalaya and the Central Range of Taiwan is not happenstance, but rather is due to the persistence of differential rock uplift rates that exceed 2 or 3 mm/a [Blythe et al., 2007; Lavé and Avouac, 2001; Whipp et al., 2007; Willett et al. 2003] and are sufficiently rapid to permit the steepened lower reach of a hanging valley to grow higher than any subsequent aggradational event that could bury it. In contrast, thermochronologic studies in the San Gabriel Mountains suggest erosion and base-level fall rates of typically < 1 mm/a [Blythe et al., 2000], whereas remnants of 90-m-thick Holocene terraces (created between 4 and 7 ka ago [Bull, 1991]) are abundant. Our modeling suggests it is unsurprising that no hanging valleys are found here: such large-scale aggradation would only have to occur once every 50–100 ka in order to bury any incipient hanging valley forming in this tectonic regime. The widespread presence of thick, Late-Glacial to Post-Glacial aggradational terraces around the world suggests that only the most rapidly deforming ranges are likely to preserve hanging valleys.

[42] Even where hanging valleys do occur, not every tributary displays a highly steepened reach at its mouth. Several factors may account for this. First, as tributary

discharges and sediment loads approach those of the main stem, their erosion capabilities should become increasingly similar. As observed in Taiwan by Wobus et al. [2006], only tributaries that are $< 10\%$ as large as the main stem catchments display hanging valleys. Second, if erosion rates were to scale with channel slope, as several formulations based on stream-power or suspended sediment loads imply, then we would not expect hanging valleys to form at all [Crosby et al., 2007; Lamb et al., 2008]. It is possible, although we think it unlikely, that adjacent drainages obey different erosion regimes, such that bed load–saltation erosion could dominate one channel and plucking could modulate an adjacent one. Third, perhaps destructive processes episodically destroy hanging valleys. As the hanging reaches grow up to 1 km high, the lithostatic stresses concentrated near their bases increase, and the underlying bedrock may become more likely to fail by fracture and landsliding [Miller and Dunne, 1996]. In this scenario, the irregular heights of hanging valleys in a compact region would simply represent the stochastic distribution of large landslides that serve to reset their heights.

10. Conclusions

[43] The presence of spectacular hanging fluvial valleys in some of the world's most rapidly eroding mountain ranges and their absence in most other settings suggest that a competition among the surface processes that create, inhibit, or destroy such valleys modulates their geographic distribution. The numerical exploration presented here predicts that (1) bed load–saltation erosion can create hanging valleys when a mismatch exists between the incision rates of a trunk channel versus its tributaries, (2) the modeled erosion rate is very sensitive to many parameters that commonly are poorly quantified, such as bed load, clast size, and flood frequency, and (3) adding in other erosion mechanisms, such as plucking, can modify the shape and height of hanging valleys, but will not necessarily inhibit their formation. Our modeling suggests that one of the simplest ways to destroy an incipient hanging valley is to cause sufficient aggradation within the trunk valley such that the steepened reach at a tributary's mouth is buried. During subsequent incision of this fill, the steepened zone is reduced back to concordance with the trunk channel. We predict that, in most mountain ranges, variations in sediment load and discharge due to climate changes cause aggradational episodes that are sufficiently large to bury and then destroy incipient hanging valleys. We observe that hanging valleys primarily form in actively deforming ranges where the rates of differential rock uplift and erosion exceed several mm/a. Such rates would permit hanging valleys to grow to heights that exceed the tops of aggradational fills formed in response to climatic variations, thereby immunizing them from the destructive effects of burial and enabling them to grow 100s of meters high.

Notation

D_s	bed load size, m.
E	rate of erosion due to bed load saltation, mm/a.
E_P	rate of erosion due to plucking, mm/a.
g	gravitational acceleration, m/s^2 .
H	water depth, m.

k	channel width power law constant.
K_P	plucking constant, mm/a.
k_v	rock resistance.
n	Manning's roughness.
Q	water discharge, m ³ /s.
Q_s	bed load supply, kg/s.
Q_t	transport capacity, kg/s.
R_b	non-dimensional buoyant density of sediment.
R_h	hydraulic radius, m.
S	channel slope.
u^*	flow shear velocity, m/s.
W	channel width, m.
w_f	settling velocity, m/s.
Y	elastic modulus.
σ_T	rock tensile strength, MPa.
τ^*	nondimensional shear stress.
τ_c^*	nondimensional critical shear stress.
τ_P^*	nondimensional critical shear stress for plucking.
ω	channel width power law exponent.

[44] **Acknowledgments.** We thank Tom Dunne, Ed Keller, and Mike Oskin for insightful discussion of this work in its early stages. We appreciate the thoughtful comments of reviewers Alex Densmore, Paul Bishop, and Noah Snyder that substantially improved the manuscript. We thank the creators of “geomorphtools.org” for freely sharing their programming. Finally, we appreciate Bodo Bookhagen for patiently sharing his expertise in channel analysis.

References

- Amos, C. B., and D. Burbank (2007), Channel width response to differential uplift, *J. Geophys. Res.*, *112*, F02010, doi:10.1029/2006JF000672.
- Attal, M., and J. Lavé (2006), Changes of bedload characteristics along the Marsyandi River (central Nepal): Implications for understanding hillslope sediment supply, sediment load evolution along fluvial networks, and denudation in active orogenic belts, *Spec. Pap. Geol. Soc. Am.*, *398*, 143–171.
- Bishop, P., T. B. Hoey, J. D. Jansen, and I. L. Artza (2005), Knickpoint recession rate and catchment area: The case of uplifted rivers in Eastern Scotland, *Earth Surf. Processes Landforms*, *30*, 767–768, doi:10.1002/esp.1191.
- Blythe, A. E., D. W. Burbank, K. A. Farley, and E. J. Fielding (2000), Structural and topographic evolution of the central Transverse Ranges, California, from apatite fission-track, (U-Th)/He and digital elevation model analysis, *Basin Res.*, *12*, 97–114, doi:10.1046/j.1365-2117.2000.00116.x.
- Blythe, A. E., D. W. Burbank, A. Carter, K. Schmidt, and J. Putkonen (2007), Plio-Quaternary exhumation history of the central Nepalese Himalaya: 1. Apatite and zircon fission track and apatite [U-Th]/He analyses, *Tectonics*, *26*, TC3002, doi:10.1029/2006TC001990.
- Bookhagen, B., R. C. Thiede, and M. R. Strecker (2005a), Abnormal monsoon years and their control on erosion and sediment flux in the high, arid northwest Himalaya, *Earth Planet. Sci. Lett.*, *231*, 131–146, doi:10.1016/j.epsl.2004.11.014.
- Bookhagen, B., R. C. Thiede, and M. R. Strecker (2005b), Late Quaternary intensified monsoon phases control landscape evolution in the northwest Himalaya, *Geology*, *33*, 149–152, doi:10.1130/G20982.1.
- Bookhagen, B., D. Fleitmann, K. Nishiizumi, M. R. Strecker, and R. C. Thiede (2006), Holocene monsoonal dynamics and fluvial terrace formation in the northwest Himalaya, India, *Geology*, *34*, 601–604, doi:10.1130/G22698.1.
- Bull, W. B. (1991), *Geomorphic Responses to Climatic Change*, 326 pp., Oxford Univ. Press, Oxford, U. K.
- Burbank, D. W., A. E. Blythe, J. Putkonen, B. Pratt-Sitaula, E. Gabet, M. Oskin, A. Barros, and T. P. Ojha (2003), Decoupling of erosion and precipitation in the Himalayas, *Nature*, *426*, 652–655, doi:10.1038/nature02187.
- Clemens, S. C., and W. L. Prell (2003), A 350,000 year summer-monsoon multi-proxy stack from the Owen Ridge, Northern Arabian Sea, *Mar. Geol.*, *201*, 35–51, doi:10.1016/S0025-3227(03)00207-X.
- Cowie, P. A., M. Attal, G. E. Tucker, A. C. Whittaker, M. Naylor, A. Ganas, and G. P. Roberts (2006), Investigating the surface process response to fault interaction and linkage using a numerical modeling approach, *Basin Res.*, *18*, 231–266, doi:10.1111/j.1365-2117.2006.00298.x.
- Crosby, B. T., and K. X. Whipple (2006), Knickpoint initiation and distribution within fluvial networks: 236 waterfalls in the Waipaoa River, North Island, New Zealand, *Geomorphology*, *82*(1–2), 16–38, doi:10.1016/j.geomorph.2005.08.023.
- Crosby, B. T., K. X. Whipple, N. M. Gasparini, and C. W. Wobus (2007), Formation of fluvial hanging valleys: Theory and simulation, *J. Geophys. Res.*, *112*, F03S10, doi:10.1029/2006JF000566.
- Dadson, S. J., et al. (2004), Earthquake-triggered increase in sediment delivery from an active mountain belt, *Geology*, *32*, 733–736, doi:10.1130/G20639.1.
- Dietrich, W. E. (1982), Settling velocity of natural particles, *Water Resour. Res.*, *18*, 1615–1626, doi:10.1029/WR018i006p01615.
- Duncan, C. C., A. J. Klein, J. G. Masek, and B. L. Isacks (1998), Comparison of Late Pleistocene and modern glacier extents in central Nepal based on digital elevation data and satellite imagery, *Quat. Res.*, *49*, 241–254, doi:10.1006/qres.1998.1958.
- Fernandez-Luque, R., and R. van Beek (1976), Erosion and transport of bed-load sediment, *J. Hydraul. Res.*, *14*, 127–144.
- Finnegan, N. J., G. Roe, D. R. Montgomery, and B. Hallet (2005), Controls on the channel width of rivers: Implications for modeling fluvial incision of bedrock, *Geology*, *33*(3), 229–232, doi:10.1130/G21171.1.
- Gabet, E. J., D. W. Burbank, B. Pratt-Sitaula, J. Putkonen, and B. Bookhagen (2008), Modern erosion rates in the High Himalayas of Nepal, *Earth Planet. Sci. Lett.*, *267*, 482–494, doi:10.1016/j.epsl.2007.11.059.
- Gasparini, N. M., K. X. Whipple, and R. L. Bras (2007), Predictions of steady state and transient landscape morphology using sediment-flux-dependent river incision models, *J. Geophys. Res.*, *112*, F03S09, doi:10.1029/2006JF000567.
- Goodbred, S. L. J., and S. A. Kuehl (1999), Holocene and modern sediment budgets for the Ganges-Brahmaputra river system: Evidence for high-stand dispersal to flood-plain, shelf, and deep-sea depocenters, *Geology*, *27*, 559–562, doi:10.1130/0091-7613(1999)027<0559:HAMSFB>2.3.CO;2.
- Hancock, G. S., and R. S. Anderson (2002), Numerical modeling of fluvial strath-terrace formation in response to oscillating climate, *Geol. Soc. Am. Bull.*, *114*, 1131–1142.
- Harp, E. L., and R. W. Jibson (1996), Landslides triggered by the 1994 Northridge, California, earthquake, *Bull. Seismol. Soc. Am.*, *86*, S319–S332.
- Kirby, E., and K. Whipple (2001), Quantifying differential rock-uplift rates via stream profile analysis, *Geology*, *29*, 415–418, doi:10.1130/0091-7613(2001)029<0415:QDRURV>2.0.CO;2.
- Lamb, M. P., W. E. Dietrich, and L. S. Sklar (2008), A model for fluvial bedrock incision by impacting suspended and bed load sediment, *J. Geophys. Res.*, *113*, F03025, doi:10.1029/2007JF000915.
- Lavé, J., and J. P. Avouac (2001), Fluvial incision and tectonic uplift across the Himalaya of central Nepal, *J. Geophys. Res.*, *106*, 26,561–26,591, doi:10.1029/2001JB000359.
- Miller, D. J., and T. Dunne (1996), Topographic perturbations of regional stresses and consequent bedrock fracturing, *J. Geophys. Res.*, *101*, 25,523–25,536, doi:10.1029/96JB02531.
- Niemi, N. A., M. Oskin, D. W. Burbank, A. M. Heimsath, and E. J. Gabet (2005), Effects of bedrock landslides on cosmogenically determined erosion rates, *Earth Planet. Sci. Lett.*, *237*, 480–498, doi:10.1016/j.epsl.2005.07.009.
- Ouimet, W., K. Whipple, L. Royden, and D. Granger (2007), Long transient response times of rivers in eastern Tibet to regional plateau uplift: The effect of mega-landslides, *Geophys. Res. Abstr.*, *7*, 05743.
- Pan, B., D. Burbank, Y. Wang, G. Wu, J. Li, and Q. Guan (2003), A 900 k.y. record of strath terrace formation during glacial-interglacial transitions in northwest China, *Geology*, *31*(11), 957–960, doi:10.1130/G19685.1.
- Playfair, J. (1802), *Illustrations of the Huttonian Theory of the Earth*, 528 pp., Cadell and Davies, London.
- Pratt, B., D. W. Burbank, A. Heimsath, and T. Ojha (2002), Impulsive alluviation during early Holocene strengthened monsoons, central Nepal Himalaya, *Geology*, *30*, 911–914, doi:10.1130/0091-7613(2002)030<0911:IADEHS>2.0.CO;2.
- Pratt-Sitaula, B. (2005), *Glaciers, Climate, and Topography in the Nepalese Himalaya*, 152 pp., Univ. of California, Santa Barbara.
- Pratt-Sitaula, B., M. Garde, D. W. Burbank, M. Oskin, A. Heimsath, and E. Gabet (2007), Bedload-to-suspended load ratio and rapid bedrock incision from Himalayan landslide-dam lake record, *Quat. Res.*, *68*(1), 111–120, doi:10.1016/j.yqres.2007.03.005.
- Sklar, L., and W. E. Dietrich (1998), River longitudinal profiles and bedrock incision models: Stream power and the influence of sediment supply, in *River Over Rock: Fluvial Processes in Bedrock Channels*, *Geophys. Monogr. Ser.*, vol. 107, edited by K. J. Tinkler and E. E. Wohl, pp. 237–260, AGU, Washington, D. C.
- Sklar, L., and W. E. Dietrich (2004), A mechanistic model for river incision into bedrock by saltating bed load, *Water Resour. Res.*, *40*, W06301, doi:10.1029/2003WR002496.

- Sklar, L., W. E. Dietrich, E. Foufuoula-Georgiou, B. Lashemes, and D. Bellugi (2006), Do gravel bed river size distributions record channel network structure?, *Water Resour. Res.*, *42*, W06D18, doi:10.1029/2006WR005035.
- Snow, R. S., and R. L. Slingerland (1987), Mathematical-modeling of graded river profiles, *J. Geol.*, *95*(1), 15–33.
- Snow, R. S., and R. L. Slingerland (1990), Stream profile adjustment to crustal warping—Nonlinear results from a simple-model, *J. Geol.*, *98*(5), 699–708.
- Snyder, N. P., K. X. Whipple, G. E. Tucker, and D. J. Merritts (2003), Importance of a stochastic distribution of floods and erosion thresholds in the bedrock river incision problem, *J. Geophys. Res.*, *108*(B2), 2117, doi:10.1029/2001JB001655.
- Tomkin, J. H., M. T. Brandon, F. J. Pazzaglia, J. R. Barbour, and S. D. Willett (2003), Quantitative testing of bedrock incision models for the Clearwater River, NW Washington state, *J. Geophys. Res.*, *108*(B6), 2308, doi:10.1029/2001JB000862.
- Whipp, D. M., T. A. Ehlers, A. E. Blythe, K. W. Huntington, K. V. Hodges, and D. W. Burbank (2007), Plio-Quaternary exhumation history of the central Nepalese Himalaya: 2. Thermokinematic and thermochronometer age prediction model, *Tectonics*, *26*, TC3003, doi:10.1029/2006TC001991.
- Whipple, K., and G. E. Tucker (2002), Implications of sediment-flux-dependent river incision models for landscape evolution, *J. Geophys. Res.*, *107*(B2), 2039, doi:10.1029/2000JB000044.
- Whipple, K. X. (2004), Bedrock rivers and the geomorphology of active orogens, *Annu. Rev. Earth Planet. Sci.*, *32*, 151–185, doi:10.1146/annurev.earth.32.101802.120356.
- Whittaker, A. C., P. A. Cowie, M. Attal, G. E. Tucker, and G. P. Roberts (2007), Bedrock channel adjustment to tectonic forcing: Implications for predicting river incision rates, *Geology*, *35*(2), 103–106, doi:10.1130/G23106A.1.
- Willett, S. D., D. Fisher, C. Fuller, Y. En-Chao, and L. C. Yu (2003), Erosion rates and orogenic-wedge kinematics in Taiwan inferred from fission-track thermochronometry, *Geology*, *31*, 945–948, doi:10.1130/G19702.1.
- Wobus, C., B. T. Crosby, and K. X. Whipple (2006), Hanging valleys in fluvial systems: Controls on occurrence and implications for landscape evolution, *J. Geophys. Res.*, *111*, F02017, doi:10.1029/2005JF000406.

D. W. Burbank and J. K. Goode, Department of Earth Science, University of California, 1006 Webb Hall, Santa Barbara, CA 93106, USA. (jgoode@crustal.ucsb.edu)